frontiers in Oncology

ORIGINAL RESEARCH
published: 27 August 2020
doi: 10.3389/fonc.2020.01668

Priming of Anti-tumor Immune Mechanisms by Radiotherapy Is Augmented by Inhibition of Heat Shock Protein 90

*Anne Ernst[1†‡], Roman Hennel[1‡], Julia Krombach[1], Heidi Kapfhammer[1], Nikko Brix[1], Gabriele Zuchtriegel[2,3], Bernd Uhl[2,3], Christoph A. Reichel[2,3], Benjamin Frey[4], Udo S. Gaipl[4], Nicolas Winssinger[5], Senji Shirasawa[6], Takehiko Sasazuki[7], Markus Sperandio[3,8], Claus Belka[1,9] and Kirsten Lauber[1,9]**

[1] Department of Radiation Oncology, University Hospital, LMU Munich, Munich, Germany, [2] Department of Otorhinolaryngology, University Hospital, LMU Munich, Munich, Germany, [3] Walter Brendel Center for Experimental Medicine, Faculty of Medicine, LMU Munich, Munich, Germany, [4] Department of Radiation Oncology, Universitätsklinikum Erlangen, Friedrich-Alexander-University Erlangen-Nürnberg (FAU), Erlangen, Germany, [5] Department of Organic Chemistry, NCCR Chemical Biology, University of Geneva, Geneva, Switzerland, [6] Department of Cell Biology, Faculty of Medicine Fukuoka University, Fukuoka, Japan, [7] Institute for Advanced Study, Kyushu University, Fukuoka, Japan, [8] Institute of Cardiovascular Physiology and Pathophysiology, Biomedical Center, LMU Munich, Munich, Germany, [9] German Cancer Consortium (DKTK), Partner Site Munich, Heidelberg, Germany

Radiotherapy is an essential part of multi-modal cancer therapy. Nevertheless, for certain cancer entities such as colorectal cancer (CRC) the indications of radiotherapy are limited due to anatomical peculiarities and high radiosensitivity of the surrounding normal tissue. The development of molecularly targeted, combined modality approaches may help to overcome these limitations. Preferably, such strategies should not only enhance radiation-induced tumor cell killing and the abrogation of tumor cell clonogenicity, but should also support the stimulation of anti-tumor immune mechanisms – a phenomenon which moved into the center of interest of preclinical and clinical research in radiation oncology within the last decade. The present study focuses on inhibition of heat shock protein 90 (HSP90) whose combination with radiotherapy has previously been reported to exhibit convincing therapeutic synergism in different preclinical cancer models. By employing *in vitro* and *in vivo* analyses, we examined if this therapeutic synergism also applies to the priming of anti-tumor immune mechanisms in model systems of CRC. Our results indicate that the combination of HSP90 inhibitor treatment and ionizing irradiation induced apoptosis in colorectal cancer cells with accelerated transit into secondary necrosis in a hyperactive Kras-dependent manner. During secondary necrosis, dying cancer cells released different classes of damage-associated molecular patterns (DAMPs) that stimulated migration and recruitment of monocytic cells *in vitro* and *in vivo*. Additionally, these dying cancer cell-derived DAMPs enforced the differentiation of a monocyte-derived antigen presenting cell (APC) phenotype which potently triggered the

OPEN ACCESS

Edited by:
Timothy F. Burns, University of Pittsburgh, United States

Reviewed by:
Phuoc T. Tran, Johns Hopkins Medicine, United States
Michele Caraglia, University of Campania Luigi Vanvitelli, Italy

***Correspondence:**
Kirsten Lauber
kirsten.lauber@med.uni-muenchen.de

†Present address:
Anne Ernst, Division of Radiation and Cancer Biology, Department of Radiation Oncology, Stanford University School of Medicine, Stanford, CA, United States

‡*These authors share first authorship*

Specialty section:
This article was submitted to Cancer Molecular Targets and Therapeutics, a section of the journal Frontiers in Oncology

Received: *10 June 2020*
Accepted: *28 July 2020*
Published: *27 August 2020*

Citation:
Ernst A, Hennel R, Krombach J, Kapfhammer H, Brix N, Zuchtriegel G, Uhl B, Reichel CA, Frey B, Gaipl US, Winssinger N, Shirasawa S, Sasazuki T, Sperandio M, Belka C and Lauber K (2020) Priming of Anti-tumor Immune Mechanisms by Radiotherapy Is Augmented by Inhibition of Heat Shock Protein 90. Front. Oncol. 10:1668. doi: 10.3389/fonc.2020.01668

priming of allogeneic T cell responses *in vitro*. In summary, HSP90 inhibition – apart from its radiosensitizing potential – obviously enables and supports the initial steps of anti-tumor immune priming upon radiotherapy and thus represents a promising partner for combined modality approaches. The therapeutic performance of such strategies requires further in-depth analyses, especially for but not only limited to CRC.

Keywords: HSP90 inhibition, radiotherapy, anti-tumor immunity, immune priming, colorectal cancer, cancer immunology, DAMPs, secondary necrosis

INTRODUCTION

Radiotherapy is a cornerstone of multi-modal cancer treatment. Its therapeutic efficacy is primarily considered to derive from direct tumor cell killing and the abrogation of tumor cell clonogenicity (1, 2). Additionally, there is growing evidence for a relevant contribution of the immune system to local as well as distant tumor control, and the concept of cancer *in situ* vaccination by radiotherapy is receiving increasing acceptance (3, 4). In this regard, the mode of cancer cell death induced by radiotherapy appears to be of fundamental importance. The priming of anti-tumor immune mechanisms has predominantly been observed in the context of necrotic forms of cell death due to the release of damage-associated molecular patterns (DAMPs) paralleled by the stimulation of an intra-tumoral type I interferon response (5, 6). Yet, the mode of irradiation-induced cell death varies considerably and depends on several factors, including the origin and genetic repertoire of the irradiated cell, the irradiation quality, the fractionation regimen, and the overall dose (4). With photon irradiation, higher single doses or strongly hypofractionated protocols, such as 3 × 8 Gy, seem to be beneficial for the stimulation of systemic anti-tumor immune mechanisms (7–10). We and others have shown that DAMPs released from irradiated, dying tumor cells stimulate the activation of endothelial cells and the recruitment of antigen presenting cells (APCs) which then crossprime $CD8^+$ T cells in a type I interferon-dependent manner involving the cGAS/STING axis (8, 9, 11–14).

Despite its broad relevance for the treatment of other solid cancer entities, indications of radiotherapy in colorectal cancer (CRC) remain largely confined to malignancies of the rectum (15–17). The increased mobility of the colon and the resulting challenges of treatment volume definition and dose administration, as well as the high degree of radiosensitivity of the surrounding normal tissue limit the application of radiotherapy in colon cancer to high-risk cases receiving adjuvant fractionated (1.8–2 Gy per fraction) or neoadjuvant hypofractionated (5 Gy per fraction) radiotherapy alone or in combination with systemic chemotherapy, respectively (16, 17). Particularly for these high-risk cases it would be of relevant clinical interest to therapeutically exploit not only the induction of tumor cell death and abrogation of clonogenicity but also the radiotherapy-induced priming of anti-tumor immune mechanisms. To this end, various combined modality approaches with molecularly targeted agents are currently being explored, including inhibition of heat shock protein 90 (HSP90) (18). The chaperone HSP90 is frequently overexpressed in tumors due to high protein turnover and constitutively increased levels of proteotoxic stress (19). It contributes to maintaining the integrity, correct folding, and stability of diverse oncogene products (20, 21). Within the large substrate spectrum, many HSP90 client proteins belong to oncogenic signaling pathways and thus orchestrate the malignant phenotype (22, 23). Hence, interference with HSP90 function appears to be a promising strategy to target cancer cells *via* multiple axes, and several HSP90 inhibitors (HSP90i) showed encouraging preclinical results (24, 25). In contrast however, most clinical trials with HSP90i monotherapy failed due to poor therapeutic efficacy and an unfavorable spectrum of side effects, particularly in terms of hepatotoxicity (26). Nevertheless, since key regulators of the DNA damage response have been reported to be specifically sensitive to HSP90i treatment, even at low inhibitor concentrations, combinations of HSP90i with radio- and/or chemotherapy recently moved into focus. The superordinate aim of these approaches is to improve the therapeutic performance and at the same time reduce the required HSP90i doses and concurrent adverse effects (27–33). For preclinical models of CRC, the radiosensitizing potential of HSP90i treatment has already been demonstrated (34, 35). We have previously shown that the second generation HSP90i NW457 exhibits reduced hepatotoxicity and potently sensitizes CRC cells toward ionizing irradiation *in vitro* and *in vivo* by interfering with the DNA damage response (36–38). The underlying mechanisms of radiation-induced cell death in the presence of HSP90i are currently being dissected (39). However, the immunological potential of HSP90i-mediated radiosensitization has not yet been examined, although seminal data suggest that HSP90i may augment the stimulation of anti-tumor immune mechanisms (19). Accordingly, the present study was designed to elucidate the immunological aspects of HSP90 inhibition in combination with ionizing irradiation in model systems of CRC. We show that the combination of radiotherapy and HSP90i treatment induced apoptosis and accelerated transit into secondary necrosis in CRC cells with concomitant release of DAMPs. These DAMPs mediated migration and recruitment of monocytic cells *in vitro* and *in vivo* and enhanced the

Abbreviations: 7-AAD, 7-amino actinomycin D; APC, antigen presenting cell; AS, autologous serum; Bax, Bcl-2-associated X protein; CFSE, carboxyfluorescein diacetate succinimidyl ester; DAMP, damage-associated molecular pattern; DC, dendritic cell; DMSO, dimethyl sulfoxide; FCS, fetal calf serum; FMI, forward migration index; GM-CSF, granulocyte-macrophage colony-stimulating factor; HMGB1, high mobility group box1; HSP, heat shock protein; HSP90i, HSP90 inhibitor; i.p., intraperitoneal; i.s., intrascrotal; IFN, interferon; IL, interleukin; Kras, Kirsten Rat Sarcoma virus protein; MLR, mixed leukocyte reaction; PI, propidium iodide; PS, penicillin/streptomycin; SDF-1α, stromal cell-derived factor 1α; TLR, toll-like receptor; TNF, tumor necrosis factor; zVAD-fmk, carbobenzoxy-valyl-alanyl-aspartyl-[O-methyl]-fluoromethylketone.

differentiation of a monocyte-derived APC phenotype which potently activated proliferation of allogeneic $CD4^+$ and $CD8^+$ T cells *in vitro*.

MATERIALS AND METHODS

Cells, Animals, and Reagents

The human CRC cell lines HCT116 $Kras^{+/G13D}$ $Bax^{+/+}$ and HCT116 $Kras^{+/G13D}$ $Bax^{-/-}$ were kindly provided by B. Vogelstein (Baltimore, MD, United States) (40), and HCT116 $Kras^{+/-}$ $Bax^{+/+}$ cells (Hke3) were a generous gift from S. Shirasawa and T. Sasazuki (Fukuoka University, Japan) (41). Cells were cultured in McCoy's full medium (McCoy's 5A medium supplemented with 10% heat-inactivated fetal calf serum (FCS) [both from Thermo Fisher Scientific, Dreieich, Germany), 100 units/ml penicillin, and 0.1 mg/ml streptomycin (PS) (Lonza, Cologne, Germany)] at 37°C and 7.5% CO_2. HCT8, HT29, and SW480 CRC cells and monocytic THP-1 cells were obtained from ATCC or DSMZ (Braunschweig, Germany) and were cultivated in DMEM full medium (DMEM (Thermo Fisher Scientific) supplemented with 10% FCS, 100 units/ml penicillin, and 0.1 mg/ml streptomycin (PS) for HCT8 and HT29 cells) at 37°C and 7.5% CO_2 or RPMI 1640 full medium [RPMI 1640 medium (Thermo Fisher Scientific) supplemented with 10% FCS, 100 units/ml penicillin, 0.1 mg/ml streptomycin (PS), and 1% 4-(2-hydroxyethyl)-1-piperazineethanesulfonic acid (HEPES, Lonza) for SW480 and THP-1 cells] at 37°C and 5% CO_2, respectively. Cell line authenticity was confirmed by short tandem repeat typing (service provided by the DSMZ), and absence of mycoplasma contamination was ensured by regular testing (MycoAlert Mycoplasma Detection Kit, Lonza).

Experiments with primary blood cells from healthy volunteers were approved by the ethics committee of the medical faculty of the LMU Munich and were performed upon written informed consent. Primary human monocytes were prepared from heparinized blood from healthy donors as described before (42) and cultured in X-Vivo full medium (X-Vivo 15 medium (Lonza) supplemented with 10% autologous serum (AS) and PS) at 37°C and 5% CO_2. Monocytes were differentiated to dendritic cells with 20 ng/ml GM-CSF and 40 ng/ml IL-4 for up to 5 days (all cytokines from R&D Systems, Wiesbaden, Germany). Naïve T cells were isolated by Biocoll density gradient centrifugation (density 1.077 g/ml, Biochrom AG, Berlin, Germany) from heparinized blood of healthy donors followed by anti-CD3 magnetic bead separation (Miltenyi, Bergisch Gladbach, Germany) according to the manufacturer's recommendations.

All *in vivo* analyses were performed in accordance with the Federation of European Laboratory Animal Science Associations (FELASA) guidelines and with the approval of local government authorities (*Regierung von Oberbayern*). Male C57BL/6 or Balb/c mice were purchased from Charles River (Sulzfeld, Germany). $CX_3CR\text{-}1^{GFP/+}$ C57BL/6 mice were generated as described previously and backcrossed for 6 to 10 generations to the C57BL/6 background (43). Mice used in the experiments were 10 to 13 weeks old and housed under standard conditions with access to food and water *ad libitum*.

The pochoxime-derived HSP90 inhibitor (HSP90i) NW457 (*epi*-pochoxime F; HSP90i) was described previously (44–46). A 10 mM stock solution was prepared in dimethyl sulfoxide (DMSO) and stored at -20°C as described (37, 38). Calcein-AM was purchased from Merck Millipore (Darmstadt, Germany), carboxyfluorescein diacetate succinimidyl ester (CFSE) from Thermo Fisher Scientific, uridine 5′-diphoshoglucose (UDP-glucose) from Abcam (Cambridge, United Kingdom), and IL-4, GM-CSF, TNF, SDF-1α, and WKYMVm (agonist of formyl-peptide receptors 1, 2, and 3) from R&D Systems. All other reagents were obtained from Sigma-Aldrich (Taufkirchen, Germany), if not stated otherwise.

Radiation Treatment and Preparation of Cell-Free, Conditioned HCT116 Cell Culture Supernatants

Cells (0.9×10^6 cells/well in a 6-well plate) were γ-irradiated with an RS225 X-ray cabinet (Xstrahl Ltd., Camberley, United Kingdom; 200 kV, 10 mA, Thoraeus filter, 1 Gy in 63 s) or with a Mueller RT-250 x-ray tube (200 kV, 10 mA, Thoraeus filter, 1 Gy in 1 min 52 s). Subsequently, full medium was replaced by serum-free medium supplemented with the indicated HSP90i concentrations. Cell-free supernatants were collected by centrifugation (10,000 × *g*, 5 min, 4°C) at the indicated time points after irradiation and stored at −80°C until further use.

Analysis of DAMPs in HCT116 Cell Culture Supernatants

HSP70, high mobility group box 1 (HMGB1) and UTP levels in cell-free supernatants were measured by ELISA (HSP70, R&D Systems; HMGB1, IBL International, Hamburg, Germany; UTP, USCN, Wuhan, China). ATP levels were analyzed by luciferase tests (ATP Determination Kit, Thermo Fisher Scientific, Waltham, MA, United States) on a Synergy MX plate reader (BioTek, Bad Friedrichshall, Germany).

Transwell Migration Assay

Transwell migration of calcein-labeled THP-1 cells toward cell-free supernatants or positive controls was allowed for 90 min with 96-well Multiscreen-MIC transwell chambers with 5 μm pore size (Merck Millipore, Darmstadt, Germany) as described before (42). Transmigrated THP-1 cells were collected by centrifugation, and transmigration was calculated from the calcein-fluorescence signal measured upon lysis on a Synergy MX plate reader (BioTek, Bad Friedrichshall, Germany) as percentage of total THP-1 cells applied.

For the biochemical characterization of monocyte attraction signals, cell-free supernatants harvested 48 h post treatment and ultracentrifuged at 42,000 × *g* (143 min, 4°C) were employed. Supernatants were subjected to heat-treatment at 90°C for 40 min, ultrafiltration with VivaSpin2 tubes with an MW cut-off of 10 kDa (Sartorius Stedim Biotech, Göttingen, Germany), or enzymatic digestion with active or heat-inactivated proteinase K

(3 U/ml) or apyrase (50 mU/ml) at 30°C for 30 min (both from New England Biolabs, Frankfurt, Germany), respectively. Culture medium supplemented with either ATP (200 nM) or SDF-1α (200 ng/ml) served as control and was treated analogously to the cell culture supernatants. Migration stimulating capacity of the processed supernatants was assessed in THP-1 cell transwell migration assays and normalized to non-treated supernatants.

Chemotaxis/Chemokinesis Assays

Chemotaxis and chemokinesis of primary human monocytes toward conditioned supernatants or apyrase digested-supernatants were analyzed with IBIDI μ-slide 2D-chemotaxis chambers (IBIDI, Munich, Germany) by live cell tracking for 3 h as described previously (42). Time-lapse video microscopy was performed on an AxioObserver Z1 inverted microscope with a heat stage (37°C, 5% CO_2) at 5 × magnification. Cell tracking was performed with ImageJ (National Institutes of Health, Bethesda, MD, United States), and cell tracks (2.5 h time frame) were analyzed with the IBIDI chemotaxis and migration tool to determine accumulated distance, Euclidean distance (linear distance between the start and end position), and forward migration index (FMI, defined as the distance from start to endpoint in gradient direction divided by the total accumulated distance).

Flow Cytometric Analyses of Apoptotic DNA Fragmentation, Plasma Membrane Integrity, and APC Surface Marker Expression

Flow cytometric measurements were performed on an LSRII cytometer (BD Biosciences, Heidelberg, Germany), and data were analyzed with FACSDiva (BD Biosciences) or FlowJo 7.6.5 Software (Tree Star Inc., Ashland, OR, United States), respectively.

Cells (4–8 × 10^4 cells/well in 24-well plate) were irradiated with 0–5 Gy in the presence of 0–625 nM HSP90i. Cells without treatment were used as controls. Time course analyses of apoptosis and necrosis induction were analyzed by flow cytometry as described previously (38). For analyses of secondary necrosis and necroptosis, the poly-caspase inhibitor zVAD-fmk (50 μM; Bachem, Bubendorf, Switzerland) or the necroptosis inhibitor necrostatin-1 (50 μM; Enzo Life Sciences, Loerrach, Germany) were used in addition to irradiation and HSP90i treatment.

For APC surface marker expression analyses, primary human monocytes (0.8–2 × 10^5 cells/well in 24-well plate) were cultured for 5 days in the presence of conditioned HCT116 culture supernatants (1 + 1 in X-Vivo full medium) with or without addition of GM-CSF (20 ng/ml) and IL-4 (40 ng/ml). 100 ng/ml TNF served as positive control. After 5 days, APCs were harvested, and stained for 20 min on ice with the following monoclonal antibodies in FACS stain buffer (BD Biosciences): anti-HLA-DR-Per-CP-Cy5.5, anti-CD86-A700, anti-CD80-PE, anti-CD40-PE-Cy5 or corresponding isotypes (all from BD Biosciences). Following two washing steps, cells were examined by flow cytometry. Expression levels of cell surface markers were calculated as median fluorescence intensities subtracted by corresponding isotype controls and are displayed as x-fold expression values compared to values obtained with HCT116 control supernatants.

Phagocytosis Assays

Phagocytosis experiments were performed as described previously (11). In brief, PKH67-labeled primary human monocytes (10^5 cells/well in a 24-well plate) were differentiated for 4 days into DCs by addition of GM-CSF (20 ng/ml) and IL-4 (40 ng/ml) and were then added to Hoechst-labeled HCT116 cells (ratio 1:2). Adherence was allowed for 4 h, and co-cultures were irradiated with 0 or 5 Gy plus 0–625 nM HSP90i treatment. After 48 h, cells were harvested by trypsinization, stained with 7-amino actinomycin D (7-AAD, BD Biosciences) for exclusion of non-viable phagocytes, and analyzed by flow cytometry. Phagocytosis was determined as percentage of 7-AAD negative, double-positive (PKH67, Hoechst) phagocytes. In order to confirm active prey cell engulfment, labeled DCs were pre-incubated with 10 μM cytochalasin D for 1 h before addition of the prey cells.

Allogeneic Mixed Leukocyte Reaction

Allogeneic mixed leukocyte reactions (MLRs) were carried out as described previously (11). Briefly, naïve CFSE-stained T cells (positively selected on anti-CD3 magnetic beads) were added in a ratio of 10:1 to allogeneic human monocyte-derived DCs (1 × 10^4 cells/well in 96-well plates) that had been differentiated in the presence of conditioned HCT116 culture supernatants in X-Vivo full medium. After 5 days, cells were collected, T cells were stained with anti-CD3-PE-Cy7, anti-CD4-PE, and anti-CD8-APC (all from BD Biosciences), and T cell proliferation was determined by flow cytometry based on the decline in T cell CFSE fluorescence intensity. Results are displayed as x-fold proliferation values normalized on the values obtained with HCT116 control supernatants.

Purinergic P2Y Receptor RT-PCR

Purinergic P2Y receptor (P2RY) expression levels were determined by RT-PCR. Total RNA was isolated from THP-1 cells and primary human monocytes with the NucleoSpin RNA II Kit according to the manufacturer's instructions, and reverse transcription was performed as described before (11). 10 ng of corresponding cDNA were subjected to amplification by PCR [10 min 95°C, 33x (15 s 95°C, 1 s 60°C)] with distinct primer pairs for each P2RY subtype (**Supplementary Table 1**). Human genomic DNA was used as positive and H_2O as negative control. Amplification products were analyzed by agarose gel electrophoresis (3% agarose gel).

Peritonitis Assays

In vivo recruitment of myeloid cells by culture supernatants of treated HCT116 cells was determined in peritonitis assays as described previously with minor variations (47–49). In brief, conditioned supernatants were injected intraperitoneally (*i.p.*) into C57BL/6 mice, and peritoneal lavages were collected from

sacrificed mice after 6 h (n = 4 per group) or after 6, 12, and 24 h (n = 2 per group) for time course analyses, respectively. Total numbers of leukocytes were determined by using a Coulter A C T counter (Beckman Coulter, Krefeld, Germany). Cells were stained on ice for 30 min with the following monoclonal antibodies: anti-CD45-APC-Cy7 (from BD Biosciences), anti-CD11b-FITC, anti-Gr-1-PE, anti-F4/80-eFluor450 (from eBiosciences, San Diego, CA, United States). FACS analyses were performed upon lysis of erythrocytes (Gallios, Beckman Coulter). Monocytic cells and granulocytes were distinguished and quantified within the $CD45^+/CD11b^+$ myeloid cell population by cell surface expression levels of Gr-1 and F4/80.

M. cremaster Assay and Intravital Microscopy

The single steps of leukocyte trafficking were examined in the *Musculus cremaster* assay by intravital microscopy as described before with minor modifications (48–51). Briefly, two groups of randomly assigned $CX_3CR1^{GFP/+}$ mice were injected intrascrotally (i.s.) and stimulated with conditioned supernatants for 6 h (n = 6 per group). After surgical preparation of the cremaster muscle, intravital microscopy was performed at an AxioTech-Vario 100 Microscope (Zeiss MicroImaging, Göttingen, Germany) equipped with a Colibiri LED light source (Zeiss MicroImaging) for fluorescence epi-illumination. Images were taken with an AxioCam Hsm digital camera with a 20 × water immersion lens (0.5 NA, Zeiss MicroImaging) and were processed with AxioVision 4.6 software (Zeiss MicroImaging). The region of interest (ROI) was analyzed with ImageJ (National Institutes of Health) for rolling, firm adhesion, and extravasation of leukocytes or $CX_3CR1^{GFP/+}$ monocytes, including classical (GFP^{low}) and non-classical monocytes (GFP^{high}), respectively. CX_3CR1-expressing DCs were excluded from analyses on the basis of their characteristic stellate morphology.

Statistical Analyses

Statistical analyses were performed using OriginPro 9.1 software (OriginLab Ltd., Northampton, MA, United States). 2-sided exact Wilcoxon Rank tests, or two-way ANOVAs were employed where indicated, and *post hoc* Bonferroni-Holm correction was applied where appropriate. Synergism was analyzed on the basis of combination indices (CIs) according to the Chou-Talalay Method (52). CIs indicate synergism (CI < 1), additivity (CI = 1), or antagonism (CI > 1).

RESULTS

HSP90i Treatment Augments Radiation-Induced Death of Colorectal Cancer Cells and the Release of Monocyte Attracting DAMPs

An initial and essential step in the induction of anti-tumor immune responses is the attraction of monocytic cells and APC precursors by dying tumor cells (53, 54). For detailed analyses of the dynamics of cell death induction and monocyte attraction, HCT116 CRC cells were irradiated at doses of 0–5 Gy in the presence of 0–625 nM HSP90i. Monocyte attraction by cell-free supernatants was measured 24–72 h after irradiation *via* transwell migration assays with the monocytic cell line THP-1. In parallel, induction of apoptosis (determined as the percentage of cells with subG1 DNA content) and necrosis (determined as the percentage of cells with permeable plasma membrane) in treated HCT116 cells was examined by flow cytometry. HSP90i strongly increased irradiation-induced apoptosis and accelerated the transit into necrosis in a dose-dependent manner (**Figure 1A**). Supernatants of dying HCT116 cells stimulated a time- and dose-dependent migratory response in THP-1 cells with a maximum approximately 48 h after treatment. Comprehensive time course analyses confirmed that monocyte attraction was strongest with supernatants harvested 48 h upon treatment with 625 nM HSP90i and 5 Gy irradiation (**Figure 1B**). Therefore, 625 nM HSP90i + 5 Gy was chosen as standard combination treatment for further experiments. Notably, combination indices calculated according to Chou and Talalay (52) revealed a synergistic mode of action for HSP90i and irradiation (CI < 1) regarding the attraction of monocytic cells.

The release of DAMPs is a vital trigger for the attraction of monocytic cells by dying tumor cells (11, 42, 53, 54). Therefore, we measured the concentrations of several established DAMPs, including HMGB1, HSP70, and ATP, in culture supernatants of HCT116 cells upon treatment. The levels of HMGB1 and HSP70 increased over time especially in response to HSP90i and combined treatment with irradiation (**Figure 1C**). Interestingly, the release of ATP into the culture supernatants revealed similar kinetics as the migratory monocyte response in the transwell assays peaking 48 h after treatment with HSP90i plus irradiation (**Figure 1B**) and exhibited also the synergistic mode of action between HSP90i and irradiation. Taken together, in comparison to the monoagent settings, combination of HSP90i and irradiation results in synergistically enhanced DAMP release and monocyte attraction by dying tumor cells.

DAMP Release and Monocyte Attraction Occur During Secondary Necrosis Upon Irradiation in Combination With HSP90i Treatment

The mode of cell death is of central importance for the stimulation of immune responses. Particularly necrotic forms of cell death – primary as well as secondary, post-apoptotic necrosis – are known to be associated with the exposure of potent immunostimulating signals (5, 6, 55). In order to assess if necrosis induction and DAMP release are a common response of CRC cells to the combined treatment of HSP90i and irradiation, we made use of three additional CRC cell lines: HCT8, SW480, and HT29 cells. Whereas HCT8 cells showed a similar response pattern as HCT116 cells, yet with elevated amplitude, neither necrosis induction nor DAMP release were observed in HT29 cells (**Supplementary Figure 1**). SW480 cells revealed an intermediate response pattern. Despite the common colorectal origin, these cell lines differ in their mutational Kras

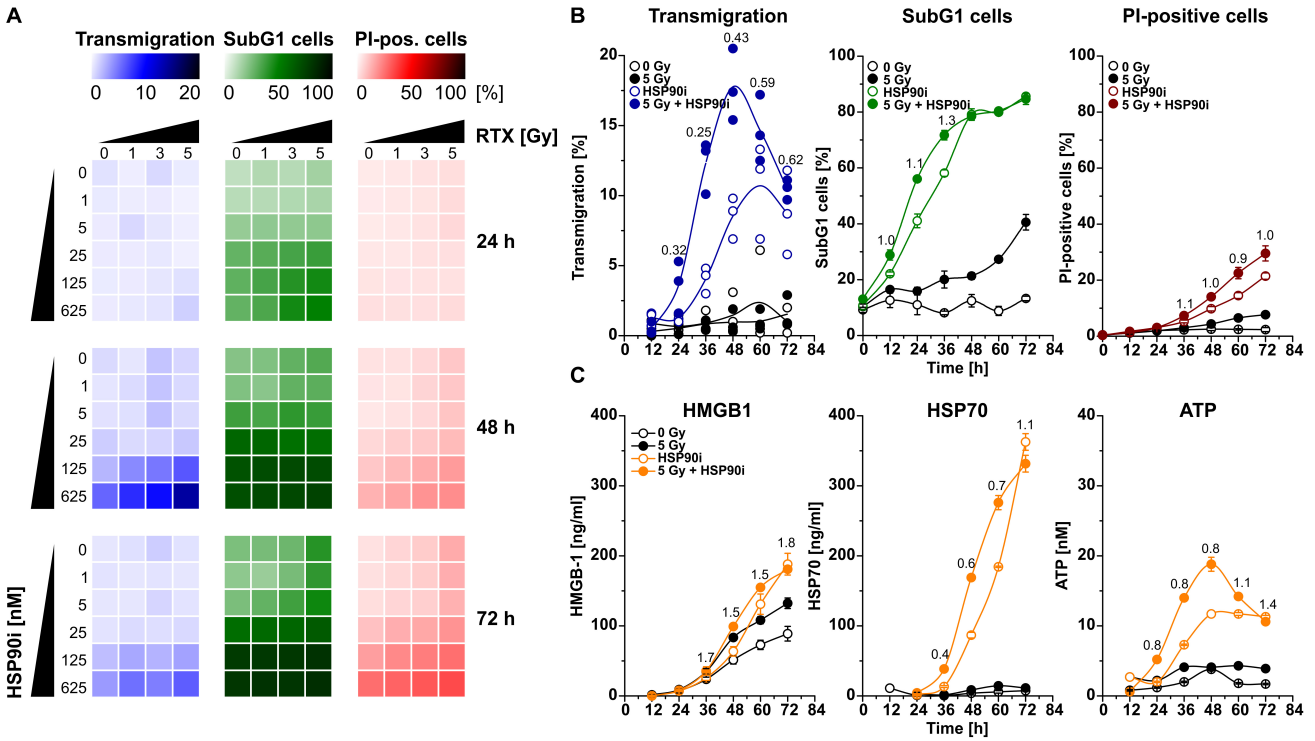

FIGURE 1 | HSP90i treatment augments radiation-induced death of colorectal cancer cells and the release of monocyte attracting DAMPs. **(A)** Transwell migration of THP-1 cells toward cell-free supernatants of HCT116 cells (left row, blue), and induction of apoptosis and necrosis in HCT116 cells (middle row, green; right row, red). HCT116 cells were irradiated with 0–5 Gy in the presence of 0–625 nM HSP90i. Cell-free supernatants of HCT116 cells were harvested at the indicated time points and subjected to transwell migration assays with monocytic THP-1 cells. Induction of apoptosis and necrosis were measured by flow cytometry of subG1 nuclei (apoptotic HCT116 cells) and propidium iodide (PI) exclusion assay (necrotic HCT116 cells). Means of $n = 3$ independent experiments are shown. **(B)** Time course of migratory stimulus release, HCT116 cell apoptosis, and necrosis induction. HCT116 cells were irradiated at 5 Gy ± 625 nM HSP90i. Untreated HCT116 cells served as controls. Transwell migration assays and detection of apoptosis and necrosis were performed as in panel **(A)**. Combination indices (CIs) are depicted. CI values <1 indicate synergism between HSP90i and irradiation. Data points of $n = 3$ independent experiments (transwell migration) or means ± SD of triplicates of one representative experiment (apoptosis and necrosis) are shown. **(C)** Time course of DAMP release. HCT116 cells were treated as in panel **(B)**. Untreated HCT116 cells served as controls. Levels of HMGB1 (left panel), HSP70 (middle panel), and ATP (right panel) were quantified in cell-free supernatants 12–72 h after treatment by ELISA (HMGB1, HSP70) or luciferase assay (ATP), respectively. Means ± SD of triplicates of one representative experiment are shown, and CIs were calculated as in panel **(B)**.

status. While HCT116 and HCT8 cells are heterozygous for hyperactive $Kras^{G13D}$, HT29 cells harbor two wildtype Kras alleles, and SW480 are homozygous for $Kras^{G12V}$ which has been shown to be associated with moderate Kras activation (56, 57). Thus, our results point toward an involvement of hyperactive $Kras^{G13D}$ in necrosis induction and DAMP release upon irradiation plus HSP90i treatment. However, since there are further molecular differences between these cell lines, we utilized isogenic subclones of HCT116 cells with genetically manipulated Kras status in order to characterize the mode(s) of cell death responsible for the observed release of monocyte attracting DAMPs in further detail. We also included HCT116 cells with manipulated Bax status to distinguish between apoptosis, primary, and secondary necrosis. So, apart from the established parental cell line HCT116 which is heterozygous for the activating Kras mutation G13D and has functional Bax, we employed HCT116 $Kras^{+/G13D}$ $Bax^{-/-}$ cells with hyperactive Kras lacking functional Bax (40) and HCT116 $Kras^{+/-}$ $Bax^{+/+}$ cells with both normal Bax and normal Kras function (41). All cell lines were treated with the combination therapy, and induction of apoptosis as well as necrosis, monocyte transwell migration, and DAMP release were monitored 0–72 h after treatment. In HCT116 parental cells, the combined treatment strongly induced apoptosis with subsequent transit into secondary necrosis, paralleled by robust monocyte attraction and release of HSP70 and ATP (**Figure 2A**, upper panel). HCT116 $Kras^{+/G13D}Bax^{-/-}$ cells, lacking the proapoptotic regulator Bax showed considerably reduced levels of apoptosis induction (**Figure 2A**, middle panel), supporting the common notion that ionizing irradiation and HSP90 inhibition stimulate apoptosis mainly *via* the intrinsic apoptosis pathway (37, 58, 59). Without preceding apoptosis, virtually no necrosis was observed in HCT116 $Bax^{-/-}$ cells, indicating that the necrotic phenotype seen in treated parental HCT116 cells was in fact of the secondary, post-apoptotic kind. Cell-free supernatants of treated HCT116 $Bax^{-/-}$ cells failed to attract monocytic cells, and only background levels of HSP70 and ATP were detected. In contrast to HCT116 $Bax^{-/-}$ cells, HCT116 $Kras^{+/-}$ $Bax^{+/+}$ cells showed a strong

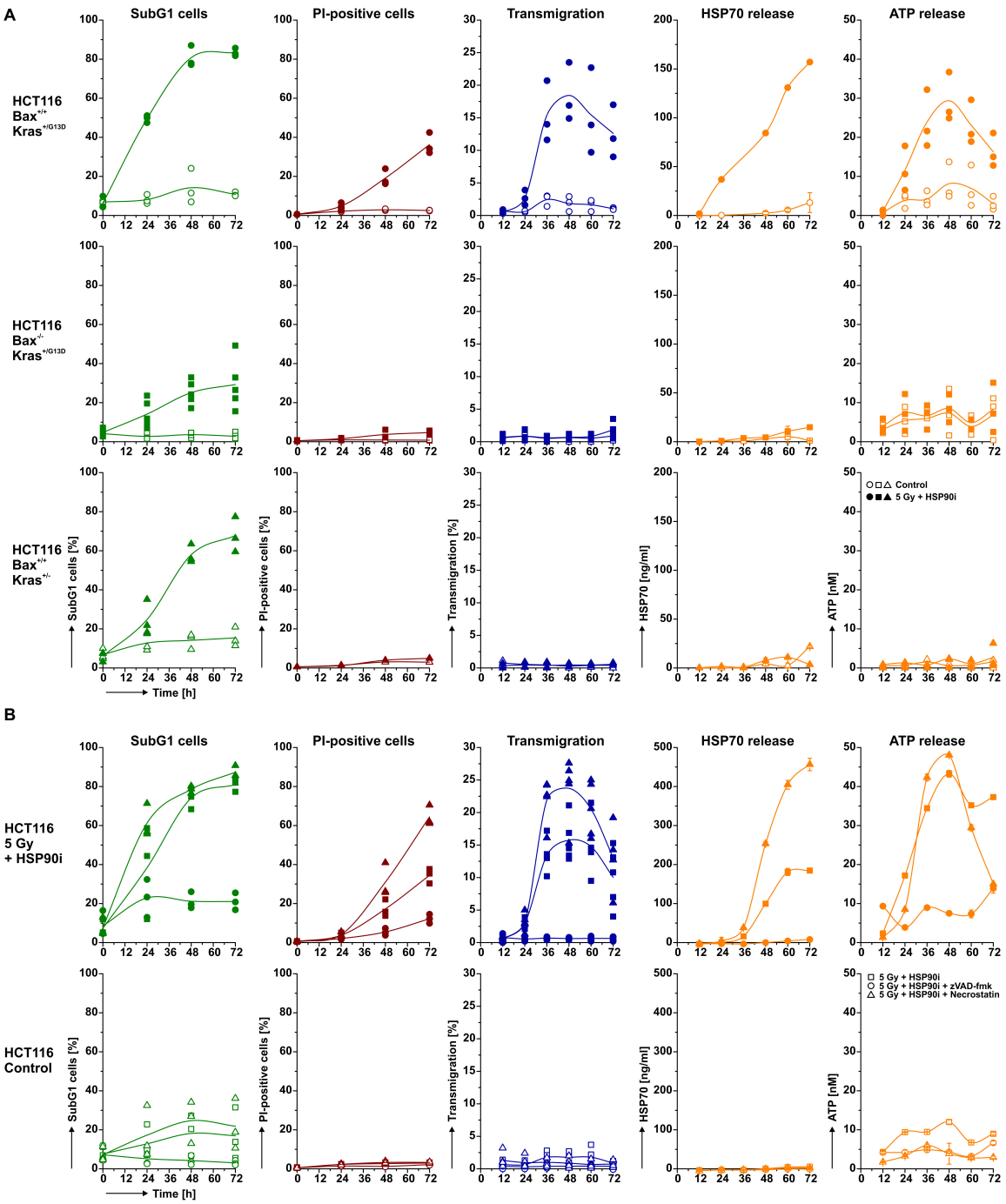

FIGURE 2 | DAMP release and monocyte attraction occur during secondary necrosis upon irradiation in combination with HSP90i treatment. **(A)** Induction of cell death, THP-1 cell attraction, and DAMP release in HCT116 subclones with or without functional Bax and/or hyperactive Kras^{G13D}. Parental HCT116 Kras$^{+/G13D}$ Bax$^{+/+}$ cells (upper row), HCT116 Kras$^{+/G13D}$ Bax$^{-/-}$ cells (middle row), and HCT116 Kras$^{+/-}$ Bax$^{+/+}$ cells (lower panel) were treated with 5 Gy plus 625 nM HSP90i or left untreated. At the indicated time points, induction of apoptosis (first column) and necrosis (second column), THP-1 cell transwell migration (third column), and release of HSP70 (fourth column) and ATP (last column) were measured as in **Figure 1**. Data points of n = 3–5 independent experiments (apoptosis, necrosis, transwell migration, ATP release) or means ± SD of triplicates of one representative experiment (HSP70 release) are shown. **(B)** Impact of different cell death inhibitors on apoptosis and necrosis induction, THP-1 cell attraction, and DAMP release in HCT116 cells upon treatment with radiotherapy and HSP90i. HCT116 cells were treated with 5 Gy plus 625 nM HSP90i in the presence of the poly-caspase inhibitor zVAD-fmk or the necroptosis inhibitor necrostatin-1, respectively (upper panel). Untreated cells served as controls (lower panel). Induction of apoptosis (first column) and necrosis (second column), THP-1 cell transwell migration (third column), and release of HSP70 (fourth column) and ATP (last column) were measured as in **Figure 1**. Data points of n = 3–5 independent experiments (apoptosis, necrosis, transwell migration) or means ± SD of triplicates of one representative experiment (release of HSP70 and ATP) are shown.

induction of apoptosis upon treatment, comparable to the parental cells (**Figure 2A**, lower panel). However, apoptotic HCT116 Kras$^{+/-}$ Bax$^{+/+}$ cells did not transit into secondary necrosis, and neither monocyte attraction nor DAMP release were observed. These results clearly suggest that DAMP release and attraction of monocytic cells after combined treatment with HSP90i and irradiation occur in the phase of post-apoptotic, secondary necrosis.

In order to further prove the causal link between monocyte attraction, DAMP release, and secondary necrosis, we employed the poly-caspase inhibitor carbobenzoxy-valyl-alanyl-aspartyl-[O-methyl]-fluoromethylketone (zVAD-fmk) which interferes with apoptosis induction and necrostatin-1, an inhibitor of receptor-interacting serine/threonine-protein kinase 1 (RIPK1), which blocks necroptosis induction *via* RIPK1 (**Figure 2B**). Addition of zVAD-fmk clearly decreased apoptosis induction in parental HCT116 cells upon treatment, subsequently also preventing transit into secondary necrosis. Consequently, neither monocyte attraction nor DAMP release were observed. In contrast, treatment with necrostatin-1 did not impair but even increased necrosis induction, eventually resulting in elevated monocyte transwell migration and HSP70 release. In summary, these data underline the essential role of secondary necrosis for the release of monocyte attracting DAMPs by dying HCT116 cells upon combined treatment with HSP90i and irradiation. Analogous results obtained with HCT8 and SW480 cells further confirmed the post-apoptotic nature of necrosis induced by irradiation plus HSP90i treatment (**Supplementary Figure 2**).

Monocyte Migration Inducing DAMPs Released Upon Irradiation Plus HSP90i Treatment Are Apyrase-Sensitive Nucleotides and Stimulate Chemokinesis *in vitro*

Necrotic cells release several DAMPs that have been reported to contribute to monocyte recruitment, including low molecular weight compounds such as nucleotides and high molecular weight compounds such as HSP70 and HMGB1 (5, 11, 42, 60). As shown in **Figures 1**, **2**, the kinetics of ATP release upon treatment of HCT116 cells with HSP90i and irradiation closely paralleled the kinetics of monocyte transwell migration, thus pointing toward a crucial contribution of nucleotides to monocyte attraction in our model system. Nevertheless, other well-known DAMPs, such as HSP70 and HMGB1, were released at high concentrations as well. In order to dissect the involvement of different molecular classes of DAMPs, the monocyte attracting signals in supernatants of treated HCT116 cells were subjected to biochemical characterization experiments. As such, heat-treatment (90°C, 40 min), ultrafiltration (molecular weight cut-off $\leq$10 kDa), and enzymatic degradation (nucleoside triphosphate degrading apyrase or protein degrading proteinase K) were applied to culture supernatants of treated HCT116 cells before THP-1 cell transwell migration was analyzed (**Figure 3A**). ATP (MW = 507 Da) and the CXC chemokine stromal cell-derived factor 1 α (SDF-1α) (MW = 11 kDa) served as controls. In summary, the migration stimulating activity in culture supernatants of HCT116 cells treated with HSP90i and irradiation was observed to be largely heat stable with an apparent molecular weight $\leq$10 kDa, and sensitive to apyrase treatment. These results indicate that nucleotides released from secondary necrotic HCT116 cells are the key players in this scenario.

Nucleotides have been reported to induce undirected forms of migration (i.e., chemokinesis) and to act as auto- and paracrine amplifiers of other chemotactic stimuli rather than stimulating directed migratory responses in monocytic cells (i.e., chemotaxis) (42, 61, 62). We therefore characterized the mode of migration of primary human monocytes stimulated by supernatants of treated HCT116 cells by live cell imaging in 2D-migration chambers in greater detail (**Figure 3B**). The chemotaxis inducing formyl peptide receptor agonist WKYMVm and chemokinesis inducing ATP were used for comparison. In response to supernatants of HCT116 cells treated with HSP90i plus irradiation, monocyte migration was clearly increased but revealed an undirected pattern as indicated by the trajectory plots and quantified by significantly increased accumulated distance while Euclidean distance and forward migration index remained not significantly different from the controls. Notably, apyrase treatment of the culture supernatants completely abrogated the chemokinetic migration of monocytic cells, thus confirming the crucial role of nucleotides in our model (**Figure 3C**). Since apyrase hydrolyzes various nucleoside triphosphates to diphosphates and monophosphates (63), a more in-depth characterization of the monocyte attracting nucleotides released from treated HCT116 cells was performed.

Migration of monocytes in response to nucleotides is mediated by the family of P2Y receptors (P2RYs) (64). RT-PCR analyses of P2RY family members showed that THP-1 cells mainly express P2RY2 and P2RY6, whereas the spectrum in primary human monocytes was broader and included P2RY2, P2RY6, P2RY12, P2RY13, and P2RY14 (**Figure 3D**). The cognate ligands of these receptors were tested for their monocyte attracting potential. Only ATP and UTP, both ligands of P2RY2, were able to stimulate transwell migration of THP-1 cells and induced chemokinesis in primary human monocytes (**Figures 3E,H**). However, whereas the concentrations of purified nucleotides needed to induce THP-1 cell migration at comparable levels to supernatants of dying HCT116 cells ranged from 125 to 1000 nM for ATP and 30–250 nM for UTP, the measured concentrations of both nucleotides in the supernatants were only in the low nanomolar range (**Figures 1**, **2**, **3F**). To characterize potential interactions between ATP and UTP, monocyte attraction was examined in checkerboard titration experiments with different concentrations of both nucleotides. The combined effects of ATP and UTP on THP-1 cell migration showed additive behavior, without obvious synergism (CI $\approx$ 1). Still, with mixtures of ATP and UTP in concentrations analogous to the ones measured in the supernatants of treated HCT116 cells (ATP 20–40 nM and UTP 20 nM) THP-1 cell migration reached comparable levels (**Figure 3G**). Accordingly, we conclude that HSP90i plus irradiation stimulates the release of the P2RY2 ligands ATP

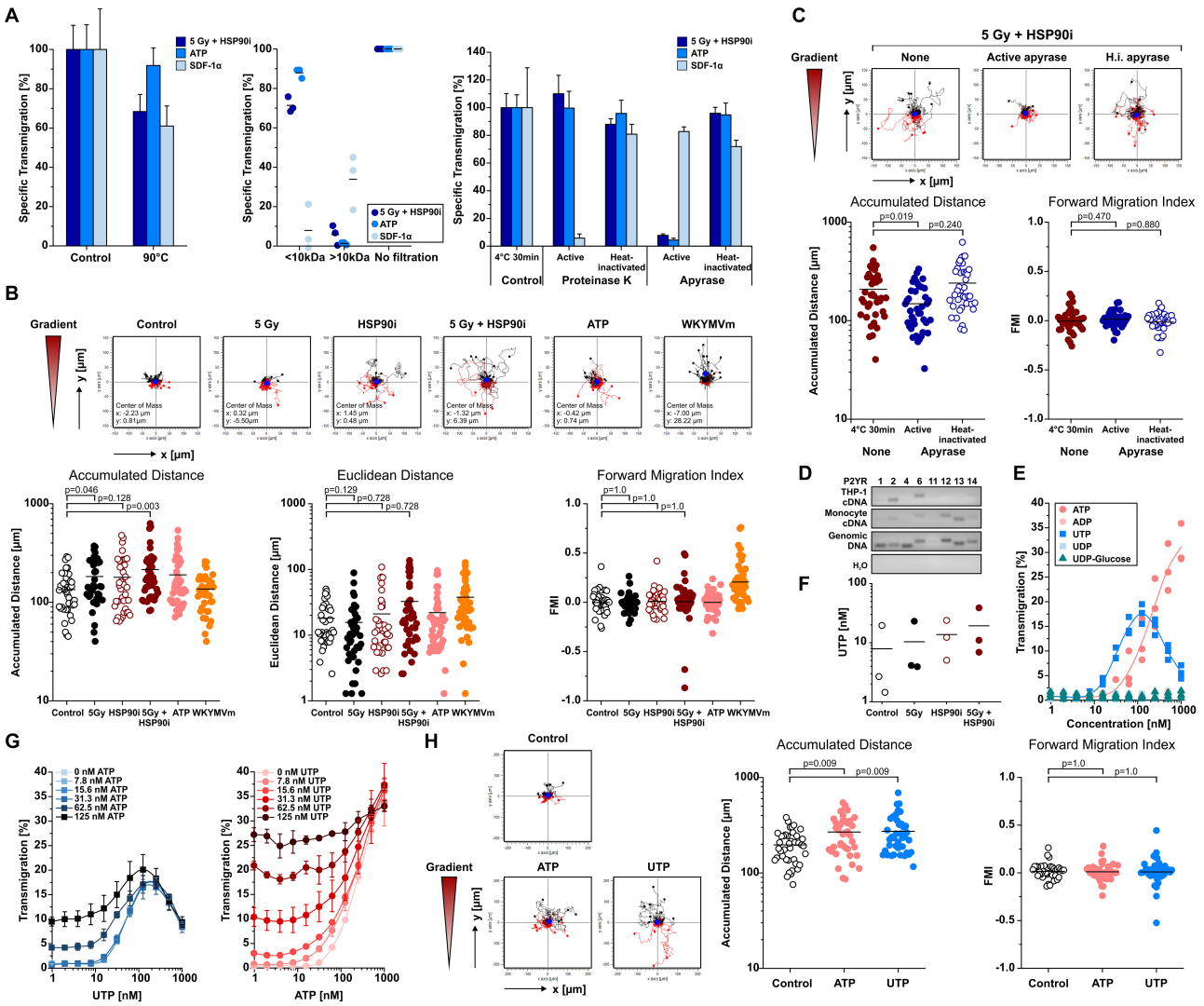

FIGURE 3 | Monocyte migration inducing DAMPs released upon irradiation plus HSP90i treatment are apyrase-sensitive nucleotides and stimulate chemokinesis *in vitro.* **(A)** Biochemical characterization of monocyte attraction signals. HCT116 cells were treated with 5 Gy plus 625 nM HSP90i. 48 h after treatment, cell- and apoptotic body-free supernatants were subjected to heat-treatment (left panel), ultrafiltration (MW cut-off 10 kDa, middle panel), or enzymatic digestion with proteinase K or apyrase, respectively (right panel). The processed supernatants were subjected to THP-1 cell transwell migration assays. Culture media supplemented with ATP (200 nM) and SDF-1α (200 ng/ml) severed as controls. THP-1 transmigration results were normalized to the values of the non-treated supernatants. Data points of $n = 3$ independent experiments (ultrafiltration) or means ± SD of quadruplicates of one representative experiment (heat treatment, enzymatic digestion) are shown. **(B)** Monocyte chemotaxis/chemokinesis. HCT116 cells were treated with 5 Gy irradiation in the absence or presence of 625 nM HSP90i. Cell-free supernatants were subjected to 2D-chemotaxis analysis, and the migratory performance of primary human monocytes was monitored by live cell tracking for 3 h (analysis window 10–160 min). Cell-free supernatants from untreated HCT116 cells, ATP (1 μM), and WKYMVm (1 μg/ml) served as controls. Trajectory plots of 40 randomly picked primary human monocytes and their corresponding centers of mass (filled blue circles) are displayed. Accumulated distance, Euclidean distance, and forward migration index (FMI) were calculated. Bars indicate mean values of 40 cells. *p*-values were calculated by 2-sided exact Wilcoxon Rank test with *post hoc* Bonferroni-Holm correction. **(C)** Biochemical characterization of monocyte chemokinesis inducing signals. Cell-free supernatants of treated HCT116 (5 Gy + 625 nM HSP90i) were digested with apyrase as in panel **(A)**. Inactivated apyrase served as control. Chemokinesis of primary human monocytes induced by processed supernatants was analyzed as in panel **(B)**. **(D)** Expression of purinergic P2Y receptors (P2RY) in THP-1 cells and primary human monocytes. P2RY subtypes were amplified from THP-1 and primary human monocyte mRNA by RT-PCR, and PCR products were separated by agarose gel electrophoresis. Human genomic DNA was used as positive and ddH_2O as negative control. **(E)** THP-1 cell transwell migration in response to different P2RY ligands. Transwell migration of THP-1 cells toward ATP, ADP, UTP, UDP, and UDP-glucose was measured in $n = 3$ independent experiments as in **Figure 1A**. **(F)** Release of UTP from HCT116 cells. HCT116 cells were irradiated with 5 Gy in the presence or absence of 625 nM HSP90i. 48 h after treatment, UTP levels were measured in cell-free supernatants by ELISA. Data points of $n = 3$ independent experiments are shown. **(G)** THP-1 cell transwell migration toward combinations of UTP and ATP. UTP (left panel) and ATP (right panel) were titrated at the indicated concentrations and THP-1 cell transwell migration was measured as in **Figure 1A**. Means ± SD of quadruplicates are displayed. **(H)** Induction of chemokinesis in primary human monocytes toward culture media supplemented with ATP (1 μM) and UTP (1 μM) was analyzed as in panel **(B)**. Non-supplemented culture medium served as control.

and UTP by HCT116 cells which trigger monocyte transwell migration in a chemokinetic way *in vitro*.

DAMPs Released Upon Irradiation Plus HSP90i Treatment Stimulate Myeloid Cell Recruitment *in vivo*

In vitro, supernatants of HCT116 cells treated with HSP90i and irradiation stimulated undirected monocyte chemokinesis. However, for the priming of anti-tumor immune mechanisms directed recruitment of APCs and their precursors, such as monocytes, is crucial (65). To examine myeloid cell recruitment by dying tumor cell-derived DAMPs *in vivo*, we used the experimental peritonitis model, one of the standard model systems to assess leukocyte trafficking *in vivo*. Culture supernatants of HCT116 cells (treated with irradiation plus HSP90i or left untreated) were injected intraperitoneally into C57BL/6 mice, and after 6 h, recruited myeloid cell populations ($CD45^+CD11b^+$) were characterized by FACS analyses of the peritoneal lavage. In comparison to the untreated controls, supernatants of treated HCT116 cells stimulated significantly enhanced infiltration of different myeloid cell subsets. This applied to classical monocytes ($Gr\text{-}1^{hi}F4/80^{hi}$ and $Gr\text{-}1^{hi}F4/80^{int}$), macrophages ($Gr\text{-}1^{low}F4/80^{hi}$), and granulocytes ($Gr\text{-}1^{hi}F4/80^{low}$) (**Figure 4A**). Time course experiments also suggested that recruited classical monocytes subsequently start to differentiate into more macrophagocytic and/or APC-like phenotypes by downregulation of Gr-1 and upregulation of F4/80 (**Figure 4B**).

To further dissect the individual steps of myeloid cell recruitment, we made use of the *M. cremaster* model, a standard microcirculatory observation technique (66). Culture supernatants of HCT116 cells (treated with irradiation plus HSP90i or left untreated) were injected intrascrotally into $CX_3CR\text{-}1^{GFP/+}$ reporter mice. After 6 hours of stimulation, the trafficking of leukocytes and GFP-positive monocytic cells from postcapillary venules into the parenchyma of the *M. cremaster* tissue was monitored by intravital microscopy. Whereas no significant differences in the initial step of leukocyte rolling were observed, firm adhesion and extravasation were significantly increased in response to supernatants of HSP90i-treated and irradiated HCT116 cells as compared to the controls. These data indicate that the myeloid cell attracting potential of DAMPs released by dying HCT116 as observed *in vitro* also translates into increased transendothelial recruitment and tissue extravasation of different myeloid subsets *in vivo*.

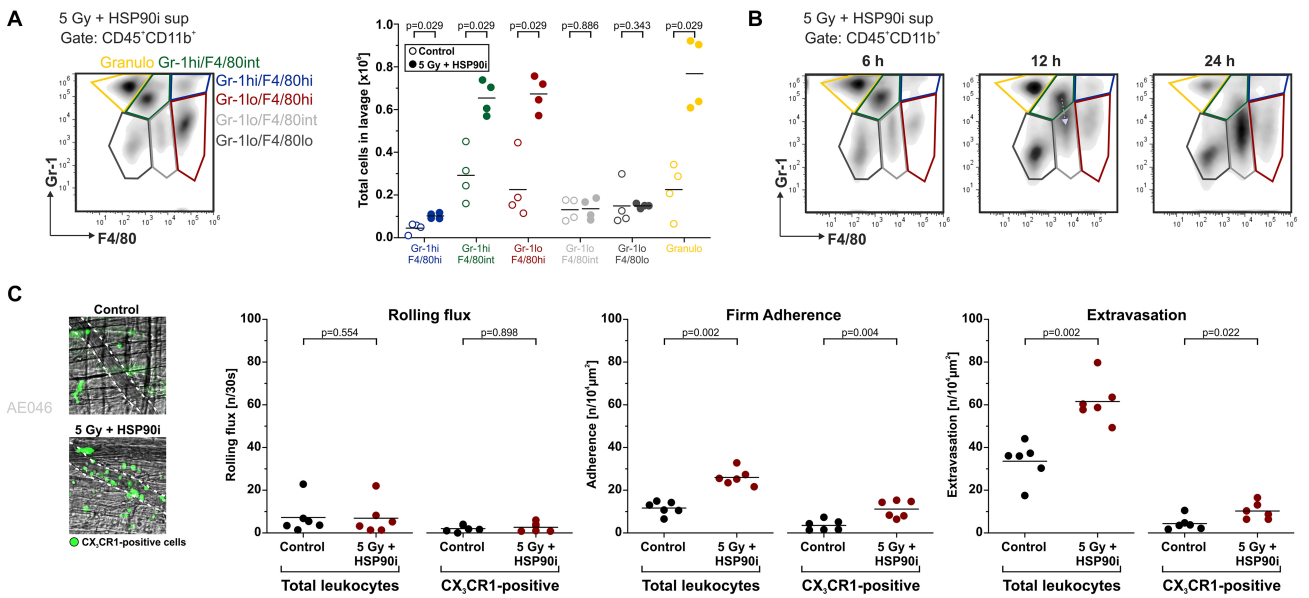

FIGURE 4 | DAMPs released upon irradiation plus HSP90i treatment stimulate myeloid cell recruitment *in vivo*. **(A)** Recruitment of myeloid leukocyte subsets in the peritonitis model. Cell-free supernatants of treated HCT116 cells (5 Gy + 625 nM HSP90i) were harvested after 48 h and injected intraperitoneally (i.p.) into C57BL/6 mice. Supernatants from untreated HCT116 cells served as controls. 6 h after injection, the peritoneal lavage was collected, and myeloid leukocyte subsets were analyzed by flow cytometry. Representative density plots of peritoneal myeloid leukocytes (Gr-1 vs. F4/80 gated on $CD45^+CD11b^+$ cells) are shown. Quantification of peritoneal recruitment is depicted for classical monocytes ($Gr\text{-}1^{hi}F4/80^{hi}$, $Gr\text{-}1^{hi}F4/80^{int}$), macrophage-like cells ($Gr\text{-}1^{low}F4/80^{hi}$, $Gr\text{-}1^{low}F4/80^{int}$, $Gr\text{-}1^{low}F4/80^{low}$), and neutrophils ($Gr\text{-}1^{hi}F4/80^{low}$). Bars indicate median values of $n = 4$ mice per group. *p*-values were calculated by two-sided exact Wilcoxon Rank test. **(B)** Time course of myeloid cell recruitment. Recruitment of myeloid leukocyte subsets was analyzed 6, 12, and 24 h after supernatant injection as in panel **(A)**. Representative density plots of $n = 2$ animals are shown. Gray arrow indicates the shift in Gr-1 expression. **(C)** Extravasation of leukocytes in the *M. cremaster* model. Cell-free HCT116 cell supernatants were generated as in panel **(A)** and intrascrotally (i.s.) injected into $CX_3CR1^{GFP/+}$ mice. Leukocyte and $CX_3CR1^{GFP/+}$ monocyte trafficking in cremasteric venules were monitored by intravital microscopy 6 hours after injection. In representative images $CX_3CR1^{GFP/+}$ monocytes are depicted in green. Intravascular rolling, firm adherence, and extravasation was quantified for total leukocytes and $CX_3CR1^{GFP/+}$ monocytes. Bars indicate mean values of $n = 6$ mice per group. *p*-values were calculated by two-sided exact Wilcoxon Rank test.

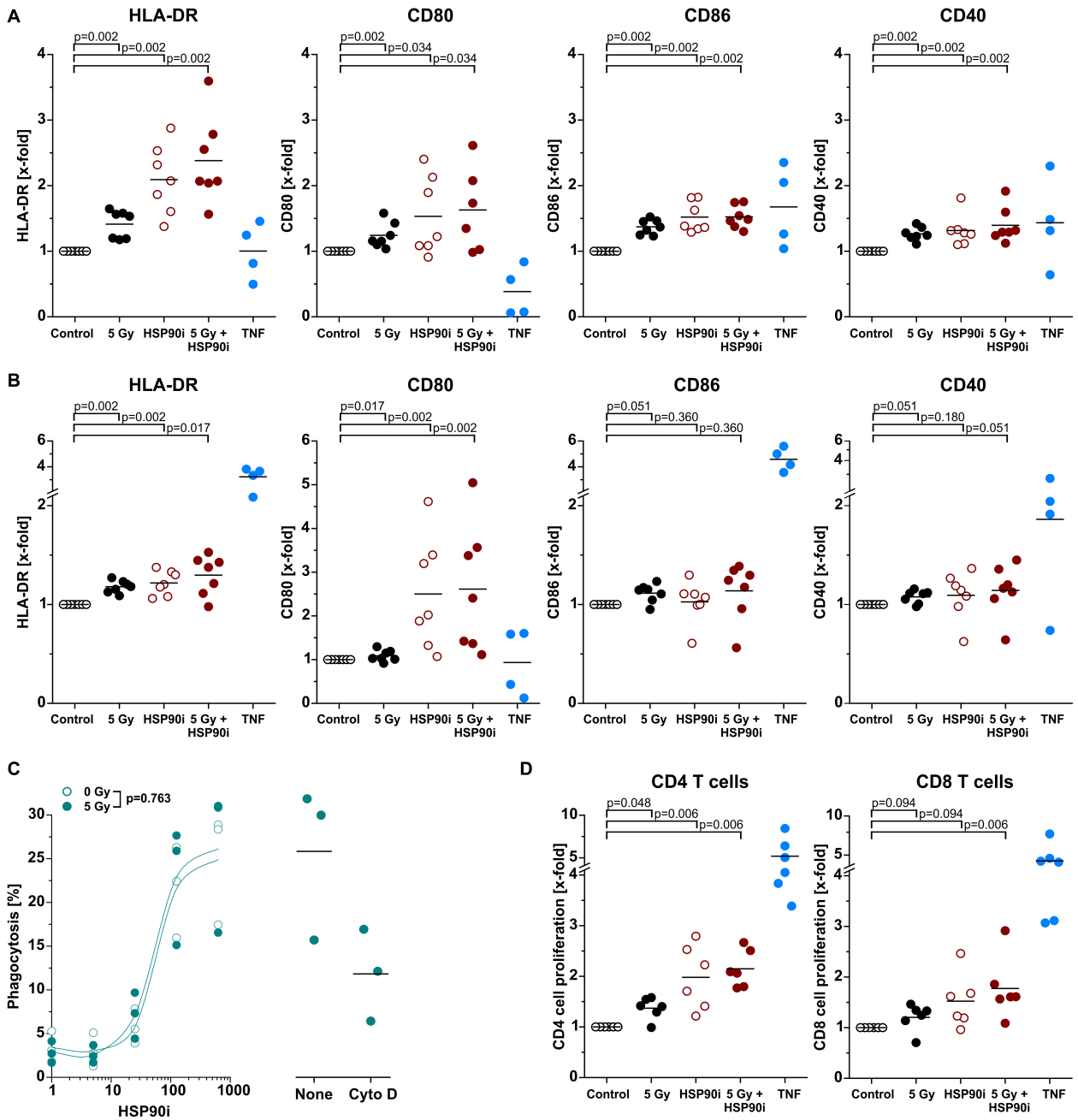

FIGURE 5 | Differentiation and effector functions of antigen presenting cells are enhanced upon contact with DAMPs released from irradiated and HSP90i-treated cancer cells. **(A)** Differentiation of antigen presenting cells from primary human monocytes. HCT116 cells were treated with 5 Gy irradiation ± 625 nM HSP90i. Cell-free supernatants were harvested 48 h after treatment, and primary human monocytes were stimulated with the supernatants (1 + 1 in X-Vivo full medium) for 5 days. Surface expression of HLA-DR, CD80, CD86, and CD40 on monocytes were analyzed by flow cytometry. Supernatants from untreated HCT116 cells and TNF served as controls. Bars indicate mean values of $n = 7$ independent experiments. p-values were calculated by two-sided exact Wilcoxon Rank test with *post hoc* Bonferroni-Holm correction. **(B)** Differentiation of monocyte-derived dendritic cells. Primary human monocytes were differentiated in the presence of GM-CSF (20 ng/ml), IL-4 (40 ng/ml), and HCT116 supernatants (1 + 1 in X-Vivo full medium), and surface marker expression was analyzed as in panel **(A)**. Bars indicate mean values of $n = 7$ independent experiments. p-values were calculated by two-sided exact Wilcoxon Rank test with Bonferroni-Holm correction. **(C)** Phagocytosis of HCT116 cells by DCs. Co-cultures of PKH67-labeled DCs [differentiated for 4 days in the presence of GM-CSF (20 ng/ml) and IL-4 (40 ng/ml)] with Hoechst-labeled dying HCT116 cells (ratio 1:2) were treated with 0 or 5 Gy + 0–625 nM HSP90i. After 48 h, phagocytosis was determined by flow cytometry as the percentage of double-positive phagocytes (left panel). Datapoints for $n = 3$ independent experiments are shown. p-values were calculated by two-way ANOVA. Treatment with 10 μM cytochalasin D was used to confirm prey cell internalization (right panel). **(D)** T cell proliferation in allogeneic mixed leukocyte reactions (MLRs). Monocyte-derived DCs differentiated as in panel **(B)** were co-cultured with CFSE-labeled allogeneic $CD3^+$ human blood T cells (ratio 1:10) for 5 days. The percentage of proliferating T cells was calculated as the percentage of $CD3^+CFSE^{low}CD4^+$ or $CD3^+CFSE^{low}CD8^+$ on the basis of all $CD3^+CD4^+$ or $CD3^+CD8^+$ cells, respectively. Bars indicate mean values of $n = 6$ independent experiments. p-values were calculated by two-sided exact Wilcoxon Rank test with Bonferroni-Holm correction.

Differentiation and Effector Functions of Antigen Presenting Cells Are Enhanced Upon Contact With DAMPs Released From Irradiated and HSP90i-Treated Cancer Cells

Upon recruitment of monocytic cells, their differentiation into potent APCs is necessary in order to achieve T cell (cross-)priming for the stimulation of systemic, adaptive anti-tumor immune responses (4, 53). Along these lines, we next exposed primary human monocytes to cell-free supernatants of treated HCT116 cells and analyzed characteristic APC surface markers of the immunological synapse by flow cytometry after 5 days without any further differentiation stimulus. As such, the MHC class II molecule HLA-DR and the co-stimulatory ligands CD80 and CD86 as well as the co-activation marker CD40 were strongly upregulated, particularly upon exposure to supernatants of HCT116 cells treated with HSP90i and irradiation, indicating differentiation into an APC phenotype (**Figure 5A**). The most robust effects were observed for CD80 and HLA-DR, and similar findings were also obtained when IL-4 and GM-CSF were additionally supplemented in order to further support APC maturation (**Figure 5B**). For successful T cell (cross-)priming, tumor antigens need to be engulfed and processed by APCs. However, in contrast to APC surface marker expression, the engulfment of treated HCT116 cells by monocyte-derived dendritic cells was not affected by irradiation and only depended on the HSP90i concentration (**Figure 5C**). Finally, we analyzed the functional relevance of enhanced APC surface marker expression for their T cell (cross-)priming capacity by allogeneic MLR with CFSE-labeled primary T cells. Priming of both, $CD4^+$ and $CD8^+$ T cell proliferation was significantly enhanced by APCs differentiated in the presence of supernatants of HSP90i-treated and irradiated HCT116 cells. Collectively, our results indicate that DAMPs released by dying HCT116 cells upon irradiation plus HSP90i treatment support the recruitment, differentiation, and T cell (cross-)priming functions of APCs, and thus should favor the stimulation of systemic anti-tumor immune responses.

DISCUSSION

Despite its central role in the medical attendance of various cancer entities, indications of radiotherapy in CRC currently remain limited to malignancies of the rectum and high-risk cases of colon cancer receiving adjuvant fractionated (1.8–2 Gy per fraction) or neoadjuvant hypofractionated (5 Gy per fraction) radiotherapy alone or in combination with systemic chemotherapy, respectively (16, 17, 67). Due to the high mobility of the colon and the relevant radiosensitivity of the surrounding normal tissue, treatment planning, target volume delineation, and dose administration remain challenging, and supporting biological approaches for specific radiosensitization of the tumor appear highly attractive. In this regard, inhibition of HSP90 has been reported to be a promising strategy. Tumor cells show a strong dependence on HSP90 chaperoning function due to their high basal protein turnover and proteotoxic stress, and crucial regulators of the DNA damage response have been identified to be particularly susceptible to HSP90 inhibition (18, 19, 22, 27). Furthermore, HSP90 in tumor cells is largely organized in multi-chaperone complexes which exhibit higher affinity for HSP90i than "normal" HSP90 complexes in non-malignant cells, thus ensuring a relevant degree of tumor specificity for HSP90i-based targeted radiosensitization (68). In this context, we and others have previously shown the synergistic therapeutic efficacy of HSP90 inhibition in combination with radiotherapy in different models of CRC *in vitro* and *in vivo* (34, 37, 39).

Apart from targeted radiosensitization, HSP90 inhibition may also enhance the priming of anti-tumor immune mechanisms that has been observed upon radiotherapy but appears to be restricted to higher single doses and strongly hypofractionated protocols (3×8 Gy) (7–11, 42). Improved priming of anti-tumor immune mechanisms would be particularly desirable for patients with high-risk CRC whose tumors are prone to local failure as well as metastasis formation, and who receive radiotherapy in fractions of $\leq$ 5 Gy – for instance in combination with immunotherapeutic protocols (69–71). Therefore, the primary motivation for our present study was to examine how HSP90 inhibition enhances radiotherapy-induced immune cell priming with the clinical perspective to develop improved treatment options for high-risk cases of colon cancer. Here, we show that HSP90 inhibition in combination with radiotherapy induced apoptosis already at radiation doses $\leq$ 5 Gy in a Bax-dependent manner and accelerated transit into secondary necrosis *via* mechanisms involving hyperactive Kras in CRC cells. During secondary necrosis, dying tumor cells released different classes of DAMPs which stimulated migration and recruitment of monocytic cells *in vitro* and *in vivo* and induced differentiation of APCs with potent antigen presenting capacity. Thus, HSP90 inhibition obviously enables and supports the initial steps of anti-tumor immune priming upon radiotherapy at radiation doses $\leq$5 Gy.

Mechanistically, our results together with prior reports reveal that HSP90i-mediated apoptosis induction upon ionizing irradiation derives from targeted disintegration of crucial DNA damage response regulators and is executed *via* the intrinsic apoptosis pathway as indicated by its clear dependence on functional Bax (37, 39). The observed accelerated transit into secondary necrosis interestingly was dependent on hyperactive Kras. Whether this observation stems from the previously reported involvement of Kras in cytoskeletal rearrangements and cell softening (72), in mechanisms of autophagy (73, 74), in metabolic rewiring (75), or so far unknown functions of hyperactive Kras, respectively, requires further investigation. Nevertheless, since a relevant number of CRC cases exhibit oncogenic Kras mutations (16), the combination of HSP90 inhibition with radiotherapy seems particularly interesting for this subgroup of patients.

In the course of secondary necrosis, dying CRC cells released different classes of DAMPs – proteins, such as HMGB1 and HSP70, as well as nucleotides, including ATP and UTP. Whereas ATP and UTP increased the chemokinetic mobility of monocytic cells in a concerted way of action as similarly described in previous studies (11, 42, 61, 62), directed recruitment of myeloid cells *in vivo* may rather rely on protein DAMPs that activate endothelial cells and stimulate the upregulation of adhesion molecules and chemokines (11, 42). Along these lines, our detailed analyses of the recruitment process in postcapillary venules in the *M. cremaster* model revealed that predominantly the steps of firm leukocyte adherence and extravasation were facilitated by DAMPs released from dying CRC cells, whereas the preceding phase of leukocyte rolling remained largely unaffected (76). This kind of activation of vascular endothelial cells allowing improved immune cell recruitment has already been described for HSP90i monotherapy settings (77).

Among the populations of myeloid cells recruited by dying CRC cell-derived DAMPs in our *in vivo* experiments, classical monocytic cells (GR-1^{hi}F4/80^{int-hi}) appear to be of specific interest for the priming of anti-tumor immune mechanisms since they have been shown to prime tumor-specific CD8$^+$ T cell responses *per se* or after intra-tumoral differentiation into potent APCs, respectively (78–80). The time-dependent decline in Gr-1 surface expression as observed in the experimental peritonitis model insinuated the differentiation into APCs (81) and was further confirmed in our *in vitro* differentiation experiments. Indeed, the upregulation of the MHC class II receptor HLA-DR, the co-stimulatory molecules CD80 as well as CD86, and the co-activating receptor CD40 upon stimulation of monocytes with supernatants of treated CRC cells indicates the emergence of a potent APC phenotype which was most pronounced upon exposure to supernatants of CRC cells treated with HSP90i plus radiotherapy. Functionally, this translated into significantly improved activation of allogeneic CD4$^+$ as well as CD8$^+$ T cells. Similar findings were obtained with supernatants of other human CRC cell lines upon irradiation with different fractionation protocols which stimulated activation of *in vitro* differentiated dendritic cells (82).

In our study, we focused on the initial steps of anti-tumor immune priming with particular interest in the release of dying cell-derived DAMPs upon radiotherapy and HSP90i treatment. Nevertheless, it should be noted that HSP90 inhibition has been described to enhance tumor immunogenicity on multiple other levels. As such, HSP90i treatment reportedly increases the expression of MHC class I and MHC class I-related molecules on tumor cells, enlarges the intracellular antigen pool, and improves the recognition of tumor cells by CD8$^+$ T cells (83, 84). Further studies observed improved T cell-dependent killing of poorly immunogenic tumor cells by HSP90 inhibition *via* additional mechanisms involving inactivation of HER2/neu, EphA2, or TCLA1, respectively (85–87). Eventually also immune checkpoint inhibition has been reported to benefit from additional HSP90 inhibition (88). However, also contradictory results describing immunosuppressive effects of HSP90i have been published (89, 90). If the HSP90i-mediated immunological effects can add to the immunogenic reconditioning of the tumor microenvironment and the stimulation of anti-tumor immunity *in vivo* which have been observed in the context of radiotherapy (91) – ideally in a synergistic manner – requires more in-depth analyses. Apparently, the therapeutic success of such approaches in the clinical situation will depend on sequence and dose of both HSP90i and radiation (4, 19, 92).

In conclusion, our study shows that the therapeutic synergism between radiotherapy and HSP90 inhibition for the treatment of CRC is not only limited to the radiosensitizing effects of HSP90 inhibition but extends also to facilitated priming of anti-tumor immune mechanisms – specifically in case of Kras-driven tumors and at clinically relevant irradiation doses $\leq$ 5 Gy. However, further studies are needed in order to optimize treatment sequence and dose, and additional immune checkpoint inhibition might be considered with the aim of achieving the best therapeutic outcome for CRC patients.

DATA AVAILABILITY STATEMENT

The raw data supporting the conclusions of this article will be made available by the authors, without undue reservation.

ETHICS STATEMENT

The studies involving human participants were reviewed and approved by Ethics Committee of the Medical Faculty of the LMU Munich. The patients/participants provided their written informed consent to participate in this study. The animal study was reviewed and approved by the Regierung von Oberbayern.

AUTHOR CONTRIBUTIONS

KL, CB, AE, RH, CR, BF, UG, NW, and MS conceived and designed the experiments. AE, RH, HK, GZ, BU, and JK performed the experiments and analyzed the data. NW provided the HSP90i NW457. SS and TS provided the HCT116 Kras$^{+/-}$ Bax$^{+/+}$ cells. AE, RH, NB, GZ, BU, and KL wrote the manuscript. All authors discussed the results and commented on the manuscript.

FUNDING

This work was supported by the DFG (SFB914 Project B06 to KL, B03 to CR, and B01 to MS, INST 409/22-1 FUGG, INST 409/20-1 FUGG, and INST 409/126-1 FUGG to CB and KL), the BMBF (ZiSS 02NUK024C and ZiSStrans 02NUK047C to KL and CB), the Elitenetzwerk Bayern (iTarget international Graduate Program), and the Wilhem-Sander-Stiftung (Project 2020.026.1 to RH).

ACKNOWLEDGMENTS

We acknowledge the iFlow Core Facility of the University Hospital Munich for assistance with the generation of flow cytometry data.

SUPPLEMENTARY MATERIAL

The Supplementary Material for this article can be found online at: https://www.frontiersin.org/articles/10.3389/fonc.2020.01668/full#supplementary-material

REFERENCES

1. Orth M, Lauber K, Niyazi M, Friedl AA, Li M, Maihofer C, et al. Current concepts in clinical radiation oncology. *Radiat Environ Biophys*. (2014) 53:1–29.
2. Citrin DE. Recent developments in radiotherapy. *N Engl J Med*. (2017) 377:2200–1. doi: 10.1056/nejmc1713349
3. Formenti SC, Demaria S. Radiation therapy to convert the tumor into an in situ vaccine. *Int J Radiat Oncol Biol Phys*. (2012) 84:879–80. doi: 10.1016/j.ijrobp.2012.06.020
4. Brix N, Tiefenthaller A, Anders H, Belka C, Lauber K. Abscopal, immunological effects of radiotherapy: narrowing the gap between clinical and preclinical experiences. *Immunol Rev*. (2017) 280:249–79. doi: 10.1111/imr.12573
5. Lauber K, Ernst A, Orth M, Herrmann M, Belka C. Dying cell clearance and its impact on the outcome of tumor radiotherapy. *Front Oncol*. (2012) 2:116. doi: 10.3389/fonc.2012.00116
6. Galluzzi L, Vitale I, Aaronson SA, Abrams JM, Adam D, Agostinis P, et al. Molecular mechanisms of cell death: recommendations of the nomenclature committee on cell death 2018. *Cell Death Differ*. (2018) 25:486–541.
7. Lee Y, Auh SL, Wang Y, Burnette B, Wang Y, Meng Y, et al. Therapeutic effects of ablative radiation on local tumor require CD8+ T cells: changing strategies for cancer treatment. *Blood*. (2009) 114:589–95. doi: 10.1182/blood-2009-02-206870
8. Lugade AA, Moran JP, Gerber SA, Rose RC, Frelinger JG, Lord EM. Local radiation therapy of B16 melanoma tumors increases the generation of tumor antigen-specific effector cells that traffic to the tumor. *J Immunol*. (2005) 174:7516–23. doi: 10.4049/jimmunol.174.12.7516
9. Lugade AA, Sorensen EW, Gerber SA, Moran JP, Frelinger JG, Lord EM. Radiation-induced IFN-gamma production within the tumor microenvironment influences antitumor immunity. *J Immunol*. (2008) 180:3132–9. doi: 10.4049/jimmunol.180.5.3132
10. Vanpouille-Box C, Alard A, Aryankalayil MJ, Sarfraz Y, Diamond JM, Schneider RJ, et al. DNA exonuclease Trex1 regulates radiotherapy-induced tumour immunogenicity. *Nat Commun*. (2017) 8:15618.
11. Krombach J, Hennel R, Brix N, Orth M, Schoetz U, Ernst A, et al. Priming anti-tumor immunity by radiotherapy: dying tumor cell-derived DAMPs trigger endothelial cell activation and recruitment of myeloid cells. *Oncoimmunology*. (2019) 8:e1523097. doi: 10.1080/2162402x.2018.1523097
12. Burnette BC, Liang H, Lee Y, Chlewicki L, Khodarev NN, Weichselbaum RR, et al. The efficacy of radiotherapy relies upon induction of type i interferon-dependent innate and adaptive immunity. *Cancer Res*. (2011) 71:2488–96. doi: 10.1158/0008-5472.can-10-2820
13. Deng L, Liang H, Xu M, Yang X, Burnette B, Arina A, et al. dna sensing promotes radiation-induced type I interferon-dependent antitumor immunity in immunogenic tumors. *Immunity*. (2014) 41:843–52. doi: 10.1016/j.immuni.2014.10.019
14. Sistigu A, Yamazaki T, Vacchelli E, Chaba K, Enot DP, Adam J, et al. Cancer cell-autonomous contribution of type I interferon signaling to the efficacy of chemotherapy. *Nat Med*. (2014) 20:1301–9.
15. Bray F, Ferlay J, Soerjomataram I, Siegel RL, Torre LA, Jemal A. Global cancer statistics 2018: GLOBOCAN estimates of incidence and mortality worldwide for 36 cancers in 185 countries. *CA Cancer J Clin*. (2018) 68:394–424. doi: 10.3322/caac.21492
16. Binefa G, Rodriguez-Moranta F, Teule A, Medina-Hayas M. Colorectal cancer: from prevention to personalized medicine. *World J Gastroenterol*. (2014) 20:6786–808. doi: 10.3748/wjg.v20.i22.6786
17. van de Velde CJ, Boelens PG, Borras JM, Coebergh JW, Cervantes A, Blomqvist L, et al. EURECCA colorectal: multidisciplinary management: European consensus conference colon & rectum. *Eur J Cancer*. (2014) 50:1.e1–e34.
18. Sveen A, Bruun J, Eide PW, Eilertsen IA, Ramirez L, Murumagi A, et al. Colorectal cancer consensus molecular subtypes translated to preclinical models uncover potentially targetable cancer cell dependencies. *Clin Cancer Res*. (2018) 24:794–806. doi: 10.1158/1078-0432.ccr-17-1234
19. Lauber K, Brix N, Ernst A, Hennel R, Krombach J, Anders H, et al. Targeting the heat shock response in combination with radiotherapy: sensitizing cancer cells to irradiation-induced cell death and heating up their immunogenicity. *Cancer Lett*. (2015) 368:209–29. doi: 10.1016/j.canlet.2015.02.047
20. Jaeger AM, Whitesell L. HSP90: enabler of cancer adaptation. *Annu Rev Cancer Biol*. (2019) 3:275–97. doi: 10.1146/annurev-cancerbio-030518-055533
21. Whitesell L, Lindquist SL. HSP90 and the chaperoning of cancer. *Nat Rev Cancer*. (2005) 5:761–72. doi: 10.1038/nrc1716
22. Trepel J, Mollapour M, Giaccone G, Neckers L. Targeting the dynamic HSP90 complex in cancer. *Nat Rev Cancer*. (2010) 10:537–49. doi: 10.1038/nrc2887
23. Hanahan D, Weinberg RA. Hallmarks of cancer: the next generation. *Cell*. (2011) 144:646–74. doi: 10.1016/j.cell.2011.02.013
24. Rozenberg P, Ziporen L, Gancz D, Saar-Ray M, Fishelson Z. Cooperation between Hsp90 and mortalin/GRP75 in resistance to cell death induced by complement C5b-9. *Cell Death Dis*. (2018) 9:150.
25. Liu K, Chen J, Yang F, Zhou Z, Liu Y, Guo Y, et al. BJ-B11, an Hsp90 inhibitor, constrains the proliferation and invasion of breast cancer cells. *Front Oncol*. (2019) 9:1447. doi: 10.3389/fonc.2019.01447
26. Yuno A, Lee MJ, Lee S, Tomita Y, Rekhtman D, Moore B, et al. Clinical evaluation and biomarker profiling of Hsp90 inhibitors. *Methods Mol Biol*. (2018) 1709:423–41. doi: 10.1007/978-1-4939-7477-1_29
27. Sharma K, Vabulas RM, Macek B, Pinkert S, Cox J, Mann M, et al. Quantitative proteomics reveals that Hsp90 inhibition preferentially targets kinases and the DNA damage response. *Mol Cell Proteomics*. (2012) 11:M111014654.
28. Kryeziu K, Bruun J, Guren TK, Sveen A, Lothe RA. Combination therapies with HSP90 inhibitors against colorectal cancer. *Biochim Biophys Acta Rev Cancer*. (2019) 1871:240–7. doi: 10.1016/j.bbcan.2019.01.002
29. Alexandrova EM, Xu S, Moll UM. Ganetespib synergizes with cyclophosphamide to improve survival of mice with autochthonous tumors in a mutant p53-dependent manner. *Cell Death Dis*. (2017) 8:e2683. doi: 10.1038/cddis.2017.108
30. Subramaniam DS, Liu SV, Crawford J, Kramer J, Thompson J, Wang H, et al. A Phase Ib/II study of ganetespib with doxorubicin in advanced solid tumors including relapsed-refractory small cell lung cancer. *Front Oncol*. (2018) 8:64. doi: 10.3389/fonc.2018.00064
31. Ray-Coquard I, Braicu I, Berger R, Mahner S, Sehouli J, Pujade-Lauraine E, et al. Part I of GANNET53: a European multicenter phase I/II trial of the Hsp90 inhibitor ganetespib combined with weekly paclitaxel in women with high-grade, platinum-resistant epithelial ovarian cancer-a study of the GANNET53 consortium. *Front Oncol*. (2019) 9:832. doi: 10.3389/fonc.2019.00832
32. Nagaraju GP, Zakka KM, Landry JC, Shaib WL, Lesinski GB, El-Rayes BF. Inhibition of HSP90 overcomes resistance to chemotherapy and radiotherapy in pancreatic cancer. *Int J Cancer*. (2019) 145:1529–37. doi: 10.1002/ijc.32227
33. Kuhnel A, Schilling D, Combs SE, Haller B, Schwab M, Multhoff G. Radiosensitization of HSF-1 knockdown lung cancer cells by low concentrations of Hsp90 inhibitor NVP-AUY922. *Cells*. (2019) 8:1166. doi: 10.3390/cells8101166
34. He S, Smith DL, Sequeira M, Sang J, Bates RC, Proia DA. The HSP90 inhibitor ganetespib has chemosensitizer and radiosensitizer activity in colorectal cancer. *Invest New Drugs*. (2014) 32:577–86. doi: 10.1007/s10637-014-0095-4
35. Spiegelberg D, Dascalu A, Mortensen AC, Abramenkovs A, Kuku G, Nestor M, et al. The novel HSP90 inhibitor AT13387 potentiates radiation effects

in squamous cell carcinoma and adenocarcinoma cells. *Oncotarget*. (2015) 6:35652–66. doi: 10.18632/oncotarget.5363
36. Whitesell L, Santagata S, Lin NU. Inhibiting HSP90 to treat cancer: a strategy in evolution. *Curr Mol Med*. (2012) 12:1108–24. doi: 10.2174/156652412803306657
37. Kinzel L, Ernst A, Orth M, Albrecht V, Hennel R, Brix N, et al. A novel HSP90 inhibitor with reduced hepatotoxicity synergizes with radiotherapy to induce apoptosis, abrogate clonogenic survival, and improve tumor control in models of colorectal cancer. *Oncotarget*. (2016) 7:43199–219. doi: 10.18632/oncotarget.9774
38. Ernst A, Anders H, Kapfhammer H, Orth M, Hennel R, Seidl K, et al. HSP90 inhibition as a means of radiosensitizing resistant, aggressive soft tissue sarcomas. *Cancer Lett*. (2015) 365:211–22. doi: 10.1016/j.canlet.2015.05.024
39. Spiegelberg D, Abramenkovs A, Mortensen ACL, Lundsten S, Nestor M, Stenerlow B. The HSP90 inhibitor onalespib exerts synergistic anti-cancer effects when combined with radiotherapy: an in vitro and in vivo approach. *Sci Rep*. (2020) 10:5923.
40. Zhang L, Yu J, Park BH, Kinzler KW, Vogelstein B. Role of BAX in the apoptotic response to anticancer agents. *Science*. (2000) 290:989–92. doi: 10.1126/science.290.5493.989
41. Shirasawa S, Furuse M, Yokoyama N, Sasazuki T. Altered growth of human colon cancer cell lines disrupted at activated Ki-ras. *Science*. (1993) 260:85–8. doi: 10.1126/science.8465203
42. Hennel R, Brix N, Seidl K, Ernst A, Scheithauer H, Belka C, et al. Release of monocyte migration signals by breast cancer cell lines after ablative and fractionated gamma-irradiation. *Radiat Oncol*. (2014) 9:85. doi: 10.1186/1748-717x-9-85
43. Jung S, Aliberti J, Graemmel P, Sunshine MJ, Kreutzberg GW, Sher A, et al. Analysis of fractalkine receptor CX(3)CR1 function by targeted deletion and green fluorescent protein reporter gene insertion. *Mol Cell Biol*. (2000) 20:4106–14. doi: 10.1128/mcb.20.11.4106-4114.2000
44. Barluenga S, Fontaine JG, Wang C, Aouadi K, Chen R, Beebe K, et al. Inhibition of HSP90 with pochoximes: SAR and structure-based insights. *Chembiochem*. (2009) 10:2753–9. doi: 10.1002/cbic.200900494
45. Barluenga S, Wang C, Fontaine JG, Aouadi K, Beebe K, Tsutsumi S, et al. Divergent synthesis of a pochonin library targeting HSP90 and in vivo efficacy of an identified inhibitor. *Angew Chem Int Ed Engl*. (2008) 47:4432–5. doi: 10.1002/anie.200800233
46. Karthikeyan G, Zambaldo C, Barluenga S, Zoete V, Karplus M, Winssinger N. Asymmetric synthesis of pochonin E and F, revision of their proposed structure, and their conversion to potent Hsp90 inhibitors. *Chemistry*. (2012) 18:8978–86. doi: 10.1002/chem.201200546
47. Lerchenberger M, Uhl B, Stark K, Zuchtriegel G, Eckart A, Miller M, et al. Matrix metalloproteinases modulate ameboid-like migration of neutrophils through inflamed interstitial tissue. *Blood*. (2013) 122:770–80. doi: 10.1182/blood-2012-12-472944
48. Uhl B, Zuchtriegel G, Puhr-Westerheide D, Praetner M, Rehberg M, Fabritius M, et al. Tissue plasminogen activator promotes postischemic neutrophil recruitment via its proteolytic and nonproteolytic properties. *Arterioscler Thromb Vasc Biol*. (2014) 34:1495–504. doi: 10.1161/atvbaha.114.303721
49. Zuchtriegel G, Uhl B, Hessenauer ME, Kurz AR, Rehberg M, Lauber K, et al. Spatiotemporal expression dynamics of selectins govern the sequential extravasation of neutrophils and monocytes in the acute inflammatory response. *Arterioscler Thromb Vasc Biol*. (2015) 35:899–910. doi: 10.1161/atvbaha.114.305143
50. Reichel CA, Uhl B, Lerchenberger M, Puhr-Westerheide D, Rehberg M, Liebl J, et al. Urokinase-type plasminogen activator promotes paracellular transmigration of neutrophils via Mac-1, but independently of urokinase-type plasminogen activator receptor. *Circulation*. (2011) 124:1848–59. doi: 10.1161/circulationaha.110.017012
51. Mempel TR, Moser C, Hutter J, Kuebler WM, Krombach F. Visualization of leukocyte transendothelial and interstitial migration using reflected light oblique transillumination in intravital video microscopy. *J Vasc Res*. (2003) 40:435–41. doi: 10.1159/000073902
52. Chou TC. Drug combination studies and their synergy quantification using the Chou-Talalay method. *Cancer Res*. (2010) 70:440–6. doi: 10.1158/0008-5472.can-09-1947
53. Chen DS, Mellman I. Oncology meets immunology: the cancer-immunity cycle. *Immunity*. (2013) 39:1–10. doi: 10.1016/j.immuni.2013.07.012
54. Kroemer G, Galluzzi L, Kepp O, Zitvogel L. Immunogenic cell death in cancer therapy. *Annu Rev Immunol*. (2013) 31:51–72.
55. Silva MT. Secondary necrosis: the natural outcome of the complete apoptotic program. *FEBS Lett*. (2010) 584:4491–9. doi: 10.1016/j.febslet.2010.10.046
56. Stolze B, Reinhart S, Bulllinger L, Frohling S, Scholl C. Comparative analysis of KRAS codon 12, 13, 18, 61, and 117 mutations using human MCF10A isogenic cell lines. *Sci Rep*. (2015) 5:8535.
57. Munoz-Maldonado C, Zimmer Y, Medova M. A comparative analysis of individual RAS mutations in cancer biology. *Front Oncol*. (2019) 9:1088. doi: 10.3389/fonc.2019.01088
58. Rudner J, Belka C, Marini P, Wagner RJ, Faltin H, Lepple-Wienhues A, et al. Radiation sensitivity and apoptosis in human lymphoma cells. *Int J Radiat Biol*. (2001) 77:1–11. doi: 10.1080/095530001453069
59. Eriksson D, Stigbrand T. Radiation-induced cell death mechanisms. *Tumour Biol*. (2010) 31:363–72. doi: 10.1007/s13277-010-0042-8
60. Sachet M, Liang YY, Oehler R. The immune response to secondary necrotic cells. *Apoptosis*. (2017) 22:1189–204. doi: 10.1007/s10495-017-1413-z
61. Isfort K, Ebert F, Bornhorst J, Sargin S, Kardakaris R, Pasparakis M, et al. Real-time imaging reveals that P2Y2 and P2Y12 receptor agonists are not chemoattractants and macrophage chemotaxis to complement C5a is phosphatidylinositol 3-kinase (PI3K)- and p38 mitogen-activated protein kinase (MAPK)-independent. *J Biol Chem*. (2011) 286:44776–87. doi: 10.1074/jbc.m111.289793
62. Kronlage M, Song J, Sorokin L, Isfort K, Schwerdtle T, Leipziger J, et al. Autocrine purinergic receptor signaling is essential for macrophage chemotaxis. *Sci Signal*. (2010) 3:ra55. doi: 10.1126/scisignal.2000588
63. Elliott MR, Chekeni FB, Trampont PC, Lazarowski ER, Kadl A, Walk SF, et al. Nucleotides released by apoptotic cells act as a find-me signal to promote phagocytic clearance. *Nature*. (2009) 461:282–6. doi: 10.1038/nature08296
64. Chen J, Zhao Y, Liu Y. The role of nucleotides and purinergic signaling in apoptotic cell clearance – implications for chronic inflammatory diseases. *Front Immunol*. (2014) 5:656.
65. Deloch L, Derer A, Hartmann J, Frey B, Fietkau R, Gaipl US. Modern radiotherapy concepts and the impact of radiation on immune activation. *Front Oncol*. (2016) 6:141. doi: 10.3389/fonc.2016.00141
66. Baez S. An open cremaster muscle preparation for the study of blood vessels by in vivo microscopy. *Microvasc Res*. (1973) 5:384–94. doi: 10.1016/0026-2862(73)90054-x
67. Hawkins AT, Ford MM, Geiger TM, Hopkins MB, Kachnic LA, Muldoon RL, et al. Neoadjuvant radiation for clinical T4 colon cancer: a potential improvement to overall survival. *Surgery*. (2019) 165:469–75. doi: 10.1016/j.surg.2018.06.015
68. Kamal A, Thao L, Sensintaffar J, Zhang L, Boehm MF, Fritz LC, et al. A high-affinity conformation of Hsp90 confers tumour selectivity on Hsp90 inhibitors. *Nature*. (2003) 425:407–10. doi: 10.1038/nature01913
69. Ghiringhelli F, Fumet JD. Is there a place for immunotherapy for metastatic microsatellite stable colorectal cancer? *Front Immunol*. (2019) 10:1816. doi: 10.3389/fimmu.2019.01816
70. Picard E, Verschoor CP, Ma GW, Pawelec G. Relationships between immune landscapes, genetic subtypes and responses to immunotherapy in colorectal cancer. *Front Immunol*. (2020) 11:369. doi: 10.3389/fimmu.2020.00369
71. Correale P, Botta C, Staropoli N, Nardone V, Pastina P, Ulivieri C, et al. Systemic inflammatory status predict the outcome of k-RAS WT metastatic colorectal cancer patients receiving the thymidylate synthase poly-epitope-peptide anticancer vaccine. *Oncotarget*. (2018) 9:20539–54. doi: 10.18632/oncotarget.24993
72. Rudzka DA, Spennati G, McGarry DJ, Chim YH, Neilson M, Ptak A, et al. Migration through physical constraints is enabled by MAPK-induced cell softening via actin cytoskeleton re-organization. *J Cell Sci*. (2019) 132:jcs224071. doi: 10.1242/jcs.224071
73. Ko A, Kanehisa A, Martins I, Senovilla L, Chargari C, Dugue D, et al. Autophagy inhibition radiosensitizes in vitro, yet reduces radioresponses in vivo due to deficient immunogenic signalling. *Cell Death Differ*. (2014) 21:92–9. doi: 10.1038/cdd.2013.124

74. Yang S, Wang X, Contino G, Liesa M, Sahin E, Ying H, et al. Pancreatic cancers require autophagy for tumor growth. *Genes Dev*. (2011) 25:717–29. doi: 10.1101/gad.2016111
75. Pupo E, Avanzato D, Middonti E, Bussolino F, Lanzetti L. KRAS-driven metabolic rewiring reveals novel actionable targets in cancer. *Front Oncol*. (2019) 9:848. doi: 10.3389/fonc.2019.00848
76. Ley K, Laudanna C, Cybulsky MI, Nourshargh S. Getting to the site of inflammation: the leukocyte adhesion cascade updated. *Nat Rev Immunol*. (2007) 7:678–89. doi: 10.1038/nri2156
77. Rao A, Taylor JL, Chi-Sabins N, Kawabe M, Gooding WE, Storkus WJ. Combination therapy with HSP90 inhibitor 17-DMAG reconditions the tumor microenvironment to improve recruitment of therapeutic T cells. *Cancer Res*. (2012) 72:3196–206. doi: 10.1158/0008-5472.can-12-0538
78. Larson SR, Atif SM, Gibbings SL, Thomas SM, Prabagar MG, Danhorn T, et al. Ly6C(+) monocyte efferocytosis and cross-presentation of cell-associated antigens. *Cell Death Differ*. (2016) 23:997–1003. doi: 10.1038/cdd.2016.24 doi: 10.1038/cdd.2016.24
79. Ma Y, Adjemian S, Mattarollo SR, Yamazaki T, Aymeric L, Yang H, et al. Anticancer chemotherapy-induced intratumoral recruitment and differentiation of antigen-presenting cells. *Immunity*. (2013) 38:729–41. doi: 10.1016/j.immuni.2013.03.003
80. Ma Y, Mattarollo SR, Adjemian S, Yang H, Aymeric L, Hannani D, et al. CCL2/CCR2-dependent recruitment of functional antigen-presenting cells into tumors upon chemotherapy. *Cancer Res*. (2014) 74:436–45. doi: 10.1158/0008-5472.can-13-1265
81. Jakubzick CV, Randolph GJ, Henson PM. Monocyte differentiation and antigen-presenting functions. *Nat Rev Immunol*. (2017) 17:349–62. doi: 10.1038/nri.2017.28
82. Kulzer L, Rubner Y, Deloch L, Allgauer A, Frey B, Fietkau R, et al. Norm- and hypo-fractionated radiotherapy is capable of activating human dendritic cells. *J Immunotoxicol*. (2014) 11:328–36. doi: 10.3109/1547691x.2014.880533
83. Fionda C, Soriani A, Malgarini G, Iannitto ML, Santoni A, Cippitelli M. Heat shock protein-90 inhibitors increase MHC class I-related chain A and B ligand expression on multiple myeloma cells and their ability to trigger NK cell degranulation. *J Immunol*. (2009) 183:4385–94. doi: 10.4049/jimmunol.0901797
84. Haggerty TJ, Dunn IS, Rose LB, Newton EE, Pandolfi F, Kurnick JT. Heat shock protein-90 inhibitors enhance antigen expression on melanomas and increase T cell recognition of tumor cells. *PLoS One*. (2014) 9:e114506. doi: 10.1371/journal.pone.0114506
85. Castilleja A, Ward NE, O'Brian CA, Swearingen B II, Swan E, Gillogly MA, et al. Accelerated HER-2 degradation enhances ovarian tumor recognition by CTL. Implications for tumor immunogenicity. *Mol Cell Biochem*. (2001) 217:21–33.
86. Kawabe M, Mandic M, Taylor JL, Vasquez CA, Wesa AK, Neckers LM, et al. Heat shock protein 90 inhibitor 17-dimethylaminoethylamino-17-demethoxygeldanamycin enhances EphA2+ tumor cell recognition by specific CD8+ T cells. *Cancer Res*. (2009) 69:6995–7003. doi: 10.1158/0008-5472.can-08-4511
87. Song KH, Oh SJ, Kim S, Cho H, Lee HJ, Song JS, et al. HSP90A inhibition promotes anti-tumor immunity by reversing multi-modal resistance and stem-like property of immune-refractory tumors. *Nat Commun*. (2020) 11:562.
88. Mbofung RM, McKenzie JA, Malu S, Zhang M, Peng W, Liu C, et al. HSP90 inhibition enhances cancer immunotherapy by upregulating interferon response genes. *Nat Commun*. (2017) 8:451.
89. Callahan MK, Garg M, Srivastava PK. Heat-shock protein 90 associates with N-terminal extended peptides and is required for direct and indirect antigen presentation. *Proc Natl Acad Sci USA*. (2008) 105:1662–7. doi: 10.1073/pnas.0711365105
90. Tsuji T, Matsuzaki J, Caballero OL, Jungbluth AA, Ritter G, Odunsi K, et al. Heat shock protein 90-mediated peptide-selective presentation of cytosolic tumor antigen for direct recognition of tumors by CD4(+) T cells. *J Immunol*. (2012) 188:3851–8. doi: 10.4049/jimmunol.1103269
91. Filatenkov A, Baker J, Mueller AM, Kenkel J, Ahn GO, Dutt S, et al. Ablative tumor radiation can change the tumor immune cell microenvironment to induce durable complete remissions. *Clin Cancer Res*. (2015) 21:3727–39. doi: 10.1158/1078-0432.ccr-14-2824
92. Jaeger AM, Stopfer L, Lee S, Gaglia G, Sandel D, Santagata S, et al. Rebalancing protein homeostasis enhances tumor antigen presentation. *Clin Cancer Res*. (2019) 25:6392–405. doi: 10.1158/1078-0432.ccr-19-0596

Conflict of Interest: *epi*-pochoxime F (NW457) has been licensed by Nexgenix Pharmaceuticals (New York, NY, United States, acquired by Oncosynergy Inc.). NW has received funding from the company and has consulted for Nexgenix Pharmaceuticals.

The remaining authors declare that the research was conducted in the absence of any commercial or financial relationships that could be construed as a potential conflict of interest.